Journal of Mathematical Modeling
Vol. -, No. -, 2026, pp. -. Research Article

JMM

Natural frequencies, longitudinal seismic vibrations and stresses of multistory buildings on a compliant foundation

Makhamatali Koraboyevich Usarov[†], Dilshod Komil ugli Shamsiyev[†], Yodgor Khurramov[‡*], Bobur Kamalov[†]

[†] *Institute of Mechanics and Seismic Stability of Structures named after M.T. Urazbaev of the Academy of Sciences of the Republic of Uzbekistan, 40 Durmon Yuli Street, 100125, Tashkent, Uzbekistan*
[‡] *TIIAME National Research University, Tashkent, Uzbekistan Kori Niyazi street 39 Kori Niyazi street*

Email(s): umakhamatali@mail.ru, dilshodshamsiyev.1993@mail.ru, yxurramov94@mail.ru, bobur514@gmail.com

Abstract. Longitudinal seismic vibrations of box-type multistory buildings are studied with a spatial continual model: the building is a thick orthotropic plate described by the bimoment theory and is coupled to a slab foundation embedded in a compliant soil. The main contribution, replacing the rigid base of earlier plate models, is this building–foundation–soil formulation: reduced moduli and density follow from the wall–slab geometry, the equations of motion are completed by contact conditions at both interfaces, and the undamped problem is solved by an explicit finite-difference scheme. For 16-story buildings the first natural frequency is 1.73–1.95 Hz ($T_1 = 0.51$–0.58 s), of the same order as the Eurocode 8 estimate for wall buildings, which is used as a reference value; time histories and frequency responses are given; at $k_c = 0.2$, $\nu_0 = 3$ Hz the peak horizontal roof displacement is 4.5–5.0 cm, considerably larger than the 2.2–2.5 cm given by an undamped fixed-base one-dimensional model.

Keywords: Multistory building, bimoment theory, thick orthotropic plate, longitudinal seismic vibration, soil–structure interaction, finite-difference method.
AMS Subject Classification 2010: 74H45, 74K20, 74S20.

1 Introduction

1.1 Statement of the problem

Box-type multistory buildings, formed by load-bearing reinforced-concrete walls and floor slabs, make up a large part of the housing stock in seismically active Central Asia. During an earthquake such a building undergoes, simultaneously, transverse bending, shear, longitudinal and torsional vibrations, and

*Corresponding author
Received: 05 May 2026/ Revised: 13 October 2026/ Accepted: 22 October 2026
DOI: 10.22124/jmm.2026.33338.3043

© 2026 University of Guilan

Corrected Proof

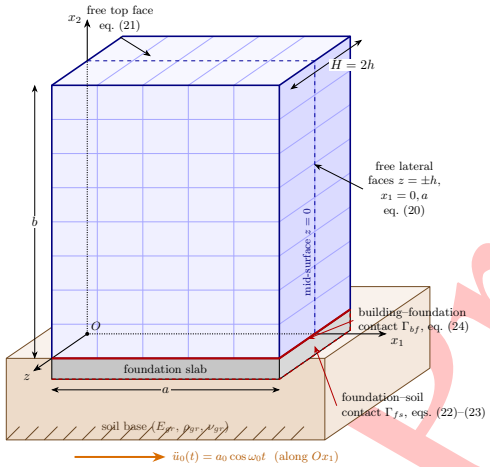

Figure 1: Problem statement: spatial continual plate model of a multistory building (length a, height b, width $H = 2h$) on a slab foundation embedded in a soil base. Coordinate system, free faces, the contact surfaces Γ_{bf} (building–foundation) and Γ_{fs} (foundation–soil) and the direction of the longitudinal ground acceleration are shown.

its deformed shape is genuinely three-dimensional. The present paper addresses one well-defined part of this problem: the *longitudinal* seismic vibrations of the building, i.e. the in-plane vibrations produced by a horizontal ground motion directed along the length of the building (axis Ox_1 in Figure 1).

The building is replaced by a continuous three-dimensional body whose outer dimensions coincide with those of the building (length a, height b, width $H = 2h$) and whose material has the *reduced* elastic moduli and density of the cellular wall–slab system (Section 2). This body is treated as a thick orthotropic plate whose mid-surface $z = 0$ is the vertical plane x_1Ox_2. The plate rests on a slab foundation which is itself embedded in a deformable soil base (Figure 1). The quantities sought are the natural frequencies, the time histories and frequency responses of the displacements, and the forces, bimoments and stresses in the building, in particular at the building–foundation interface where the largest stresses occur. The problem is posed on four types of boundaries: the free top face, the free lateral faces, the building–foundation contact surface Γ_{bf} and the foundation–soil contact surface Γ_{fs}.

1.2 Literature review and research gap

One-dimensional and discrete models. The classical approach reduces a building to a one-dimensional member. Vlasov [33] introduced the bimoment to describe non-uniform torsion and warping of thin-walled beams; applied to a whole building, this theory remains one-dimensional and does not describe the deformation of the building across its thickness. Clough and Penzien [7] and Chopra [6] represent the building by a lumped-mass multi-degree-of-freedom (MDOF) system or by a continuous cantilever beam, under the hypotheses of rigid floor diaphragms and plane cross-sections. Stafford Smith and Coull [24] systematised continuum (shear–flexural beam) methods for tall buildings, and Miranda and Taghavi [20] used a coupled shear–flexural beam to estimate floor-acceleration demands with a single stiffness parameter. Wdowicki et al. [34] combined a continuous stiffness model with discrete floor masses for irregular shear-wall buildings. These models are efficient, but by construction they cannot give the distribution of stresses across the width of the building or the local stresses at wall intersections

Corrected Proof

and at the foundation.

Three-dimensional numerical models and design-oriented studies. Detailed finite-element models are the standard tool in design. Abaev et al. [1] compared five structural systems of 20-story buildings with such models, Abdel Raheem et al. [2] showed that plan irregularity increases seismic demands, Rigato and Medina [23] and Ghersi and Rossi [12] studied the effect of the incidence angle of bidirectional ground motion, and El-Betar [9] proposed a procedure for the vulnerability evaluation of existing buildings. Full finite-element models, however, are expensive for parametric and resonance studies in which the excitation frequency is swept over a wide range, as is done in Section 6.

Higher-order plate theories. Between one-dimensional models and full 3D analysis lie two-dimensional theories of thick plates. Mindlin [19] added transverse shear and rotary inertia to plate theory, Reddy [22] introduced a third-order displacement field that satisfies traction-free conditions on the faces, and Ike [13] recently derived a third-order formulation from first principles. The bimoment theory of thick plates [21, 26] belongs to this family but does not rely on an assumed displacement field: the three-dimensional equations of elasticity are integrated over the thickness, the face conditions are approximated by Maclaurin series with eight terms per displacement component, and the forces, moments and *bimoments* are expressed exactly through nine generalized functions of two coordinates and time.

Soil–structure interaction (SSI). Wolf [35] and Stewart et al. [25] established that foundation compliance lengthens the natural periods of a building and changes its response relative to a fixed base. Recent studies confirm this for asymmetric frames [5], for combined bracing/shear-wall systems [15], for neighbouring inelastic buildings [32], and at larger scales [14]. In these works the building is modelled by beams, frames or finite elements; SSI has not been combined with a thick-plate model of the whole building.

Continual plate models of buildings. Our group has developed a continual plate model of box-type buildings [4, 28, 30]: the building is treated as a thick orthotropic plate with reduced moduli, and its vibrations are described by the bimoment theory. The model has been applied to transverse vibrations [30, 31] and to longitudinal vibrations [17, 27]; in all these studies the building is *rigidly fixed* at its base, and the foundation and soil are not modelled.

Research gap. In summary, one-dimensional and MDOF models do not resolve the through-thickness stress distribution, full finite-element models are too costly for frequency sweeps, SSI studies do not use a thick-plate model of the building, and the existing plate-model studies assume a rigid base. A computationally efficient model that describes the spatial (through-thickness) stress state of the building *and* its interaction with the foundation and soil under longitudinal seismic action is therefore lacking. The present paper fills this gap.

1.3 Novelty with respect to the authors' previous work

The differences between this paper and our earlier publications [17, 27, 29, 31] are summarised in Table 1. Paper [31] formulated the layered plate model and solved the problem of *transverse* vibrations with an absolutely rigid foundation. Paper [29] applied the plate model to seismic vibrations of buildings on a rigid base. Papers [17, 27] treated *longitudinal* vibrations but with the base displacement prescribed, $\overline{u}_1(x_1, 0, t) = u_0(t)$, i.e. without a foundation, and reported only natural frequencies and peak values. The present paper is the first to (i) couple the plate model of the building to a slab foundation and a soil base through the contact conditions (22)–(24); (ii) introduce the local stresses $\sigma^*_{13}, \sigma^*_{23}, \sigma^*_{33}$ at wall intersections (16); (iii) give time histories and frequency-response curves; and (iv) compare the results

Corrected Proof

Table 1: Relation of the present study to the authors' previous plate-model publications

Study	Vibration problem	Base / foundation	Output	Comparison
[31] (2023)	transverse	rigid foundation	frequencies, stresses	–
[17] (2023), [27] (2024)	longitudinal	prescribed base motion (no foundation)	frequencies, peak displacements and stresses	–
[29] (2025)	seismic, plate model	rigid base	displacements, stresses	–
Present paper	longitudinal	slab foundation + compliant soil, contact conditions (22)–(24)	frequencies, time histories, frequency response, forces, bimoments, local stresses σ_{ij}^{*}	code formulas, 1D modal model, literature

with code period formulas, used as reference values, and with a classical modal model.

1.4 Contributions and organisation of the paper

The main contributions of the paper are:

(i) closed-form reduced elastic moduli, shear moduli and density of the continual model, obtained from the cellular wall–slab geometry of the building (Section 2);

(ii) a complete boundary-value problem for the longitudinal vibrations of the building–foundation–soil system, consisting of three coupled systems of equations for forces, bimoments and compressive bimoments, with boundary conditions on the free faces and contact conditions at Γ_{bf} and Γ_{fs} (Sections 3–4);

(iii) an explicit finite-difference scheme for the undamped problem with a stated Courant-type stability condition (Section 5);

(iv) natural frequencies, time histories, frequency-response curves, displacements and stresses of 16-story buildings of three widths (Section 6);

(v) comparison with code period formulas, ambient-vibration data and a classical one-dimensional modal model (Section 7).

Section 8 gives the conclusions.

2 Reduced elastic moduli, shear moduli and density of the continual model

The longitudinal vibration problem is the symmetric problem of the bimoment theory of plates [21, 26]. The building is referred to the Cartesian system x_1, x_2, z, with Ox_1 along the length, Ox_2 along the height and Oz along the width of the building (Figure 1). The reduction method below follows [4, 26]; it is a homogenisation of the cellular structure in the sense of the continuum methods for tall buildings [24]. The building is regarded as a parallelepiped divided by walls and slabs into a large number of cells (rooms).

Let E_0, G_0, ν_{w} and ρ_0 be the elastic modulus, shear modulus, Poisson ratio and density of the wall material (reinforced concrete); the Poisson ratio is denoted ν_{w} to distinguish it from the excitation frequency ν_0 of Section 6. For the continual model, E_1, E_2, E_3 are the reduced elastic moduli, G_{12}, G_{13}, G_{23} the reduced shear moduli, $\nu_{12}, \nu_{13}, \nu_{23}$ the Poisson ratios and ρ the reduced density. The geometric data are the width $H = 2h$, the plan dimensions a, b, the thickness h_1 of the external walls, the thickness h_2

Corrected Proof

of the internal walls, the thickness h_3 of the floor slabs, the spacings a_1 and c_1 of the transverse and longitudinal walls, and the story height b_1 (Figures 2 and 3); N_s denotes the number of stories, so that $b = N_s b_1$.

The reduced characteristics are

$$\begin{aligned} &E_1 = \alpha\,\xi_{11}\,E_0, \quad E_2 = \alpha\,\xi_{22}\,E_0, \quad E_3 = \alpha\,\xi_{33}\,E_0, \\ &G_{12} = \alpha\,\xi_{12}\,G_0, \quad G_{13} = \alpha\,\xi_{13}\,G_0, \quad G_{23} = \alpha\,\xi_{23}\,G_0, \quad \rho = \alpha\,\zeta_0\,\rho_0, \end{aligned} \tag{1}$$

where ξ_{ij} and ζ_0 are dimensionless reduction coefficients and α is a coefficient of the cellular structure,

$$\alpha = \sqrt{\frac{\sqrt{a_1 b_1}}{2(a_1 + b_1)}}. \tag{2}$$

Because a story consists mostly of air enclosed by a sparse lattice of walls and slabs, its smeared stiffness and inertia are only a fraction of those of concrete; this fraction is given by ξ_{ij}, ζ_0 and α. A long, low cell (large a_1/b_1 or b_1/a_1) gives a smaller α than a square cell of the same area.

The reduction coefficients are area and volume fractions of solid material:

$$\xi_{11} = \frac{F_{11}}{F_{01}}, \quad \xi_{22} = \frac{F_{22}}{F_{02}}, \quad \xi_{33} = \frac{F_{33}}{F_{03}}, \quad \xi_{12} = \frac{2h_1 + h_2}{H}, \quad \xi_{13} = \frac{h_3}{b_1}, \quad \xi_{23} = \frac{h_2}{a_1}, \quad \zeta_0 = \frac{V_1}{V_0}, \tag{3}$$

where F_{01}, F_{02}, F_{03} are the areas of the sections of one story by the three coordinate planes and F_{11}, F_{22}, F_{33} are the areas of walls and slabs in these sections:

$$\begin{aligned} &F_{01} = b_1 H, \qquad F_{02} = aH, \qquad F_{03} = b_1 a, \qquad F_{11} = b_1 h_2 + H h_3, \\ &F_{22} = 2H h_1 + (n-1) H h_2 + 2a h_1 + a h_2, \qquad F_{33} = a h_2 + 2 b_1 h_1 + (n-1) b_1 h_2, \end{aligned} \tag{4}$$

n being the number of internal transverse walls in a story. V_0 is the volume of one story and V_1 the volume of its walls and slabs:

$$V_1 = 2ab_1 h_1 + a b_1 h_2 + 2H b_1 h_1 + (n-1) H b_1 h_2 + aH h_3, \qquad V_0 = abH. \tag{5}$$

According to (1)–(5), the reduced elastic moduli of the continual model are 10–30 times smaller than the modulus of the wall panels, and the reduced density is 8–15 times smaller than the density of the panel material, which reflects the large share of voids in a story.

For the orthotropic body, Hooke's law is [16]

$$\begin{aligned} &\sigma_{11} = E_{11}\varepsilon_{11} + E_{12}\varepsilon_{22} + E_{13}\varepsilon_{33}, \qquad \sigma_{22} = E_{21}\varepsilon_{11} + E_{22}\varepsilon_{22} + E_{23}\varepsilon_{33}, \\ &\sigma_{33} = E_{31}\varepsilon_{11} + E_{32}\varepsilon_{22} + E_{33}\varepsilon_{33}, \qquad \sigma_{12} = 2G_{12}\varepsilon_{12}, \quad \sigma_{13} = 2G_{13}\varepsilon_{13}, \quad \sigma_{23} = 2G_{23}\varepsilon_{23}, \end{aligned} \tag{6}$$

with

$$\begin{aligned} &E_{11} = E_1 g_{11}, \qquad E_{22} = E_2 g_{22}, \qquad E_{33} = E_3 g_{33}, \\ &E_{12} = E_{21} = E_1 g_{12} = E_2 g_{21}, \quad E_{13} = E_{31} = E_1 g_{13} = E_3 g_{31}, \quad E_{23} = E_{32} = E_2 g_{23} = E_3 g_{32}, \end{aligned} \tag{7}$$

$$\begin{aligned} &g_{11} = \frac{1 - \nu_{23}\nu_{32}}{1 - \mu^2}, \qquad g_{22} = \frac{1 - \nu_{13}\nu_{31}}{1 - \mu^2}, \qquad g_{33} = \frac{1 - \nu_{12}\nu_{21}}{1 - \mu^2}, \\ &g_{12} = g_{21} = \frac{\nu_{12} + \nu_{13}\nu_{32}}{1 - \mu^2}, \qquad g_{13} = g_{31} = \frac{\nu_{13} + \nu_{12}\nu_{23}}{1 - \mu^2}, \qquad g_{23} = g_{32} = \frac{\nu_{23} + \nu_{13}\nu_{21}}{1 - \mu^2}, \\ &\mu^2 = \nu_{12}\nu_{21} + \nu_{23}\nu_{32} + \nu_{13}\nu_{31} + 2\nu_{12}\nu_{23}\nu_{31}. \end{aligned} \tag{8}$$

Corrected Proof

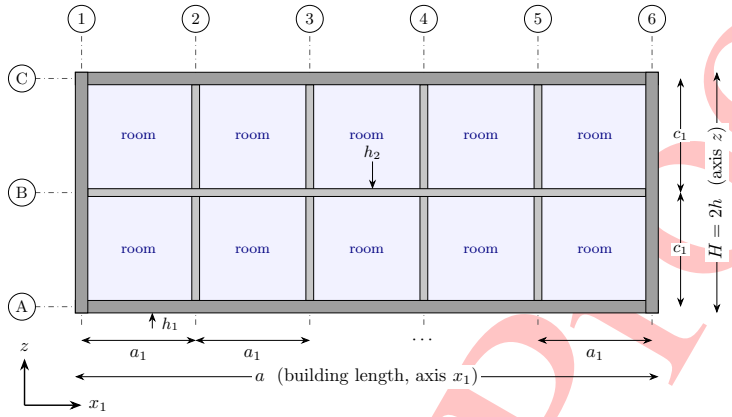

Figure 2: Plan of the cellular box model: transverse walls on grid lines 1–6 with spacing a_1, longitudinal walls A, B, C with spacing c_1, external wall thickness h_1, internal wall thickness h_2

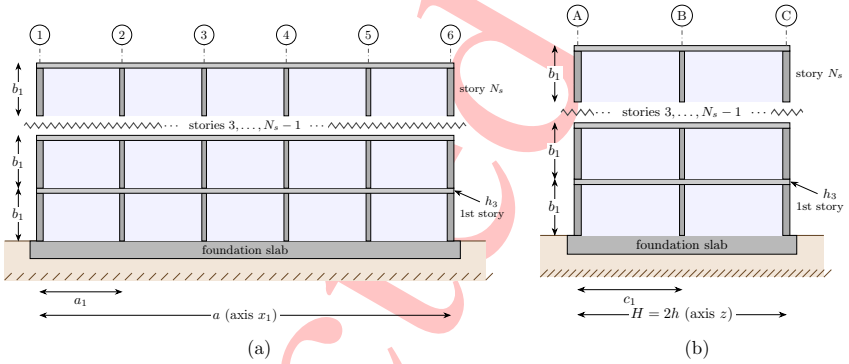

Figure 3: Sections of the cellular box model (three of the N_s stories are shown): (a) longitudinal section with wall spacing a_1 along grid lines 1–6; (b) transverse section with width H and longitudinal walls A, B, C; b_1 is the story height and h_3 the slab thickness

3 Generalized displacements, forces and bimoments

Following the bimoment theory of thick plates [21,26], the displacements u_1, u_2, u_3 of the three-dimensional body are represented by their face values and by weighted integrals over the thickness. In contrast to the theories of Mindlin [19] and Reddy [22], no displacement field is assumed; the through-thickness moments are defined exactly and the face conditions are approximated by Maclaurin series with eight terms per component [26]. The longitudinal problem involves nine generalized functions:

$$\begin{aligned}
\overline{u}_1 &= \frac{u_1^{(+)} + u_1^{(-)}}{2}, \quad \overline{\psi}_1 = \frac{1}{2h}\int_{-h}^{h} u_1\, dz, \quad \overline{\beta}_1 = \frac{1}{2h^3}\int_{-h}^{h} u_1 z^2\, dz, \\
\overline{u}_2 &= \frac{u_2^{(+)} + u_2^{(-)}}{2}, \quad \overline{\psi}_2 = \frac{1}{2h}\int_{-h}^{h} u_2\, dz, \quad \overline{\beta}_2 = \frac{1}{2h^3}\int_{-h}^{h} u_2 z^2\, dz, \\
\overline{W} &= u_3^{(+)} - u_3^{(-)}, \quad \overline{r} = \frac{1}{2h^2}\int_{-h}^{h} u_3 z\, dz, \quad \overline{\gamma} = \frac{1}{2h^4}\int_{-h}^{h} u_3 z^3\, dz,
\end{aligned} \tag{9}$$

Corrected Proof

where $u_i^{(\pm)}$ are the displacements of the faces $z=\pm h$. The functions $\overline{\psi}_i$ are mean displacements, while $\overline{\beta}_i, \overline{r}, \overline{\gamma}$ describe the warping of the cross-section (Figure 4); they vanish in any theory, such as beam and shear-type MDOF models, in which the cross-section remains plane. All nine generalized functions have the dimension of length (m). The load terms are

$$\overline{q}_1 = \frac{q_1^{(+)} - q_1^{(-)}}{2}, \qquad \overline{q}_2 = \frac{q_2^{(+)} - q_2^{(-)}}{2}, \qquad \overline{q}_3 = \frac{q_3^{(+)} + q_3^{(-)}}{2}. \tag{10}$$

The forces associated with $\sigma_{11}, \sigma_{22}, \sigma_{12}$ are

$$\begin{aligned} N_{11} &= \int_{-h}^{h} \sigma_{11}\, dz = H\left(E_{11}\frac{\partial \overline{\psi}_1}{\partial x_1} + E_{12}\frac{\partial \overline{\psi}_2}{\partial x_2} + E_{13}\frac{2\overline{W}}{H}\right), \\ N_{22} &= \int_{-h}^{h} \sigma_{22}\, dz = H\left(E_{12}\frac{\partial \overline{\psi}_1}{\partial x_1} + E_{22}\frac{\partial \overline{\psi}_2}{\partial x_2} + E_{23}\frac{2\overline{W}}{H}\right), \\ N_{12} &= N_{21} = \int_{-h}^{h} \sigma_{12}\, dz = G_{12}H\left(\frac{\partial \overline{\psi}_1}{\partial x_2} + \frac{\partial \overline{\psi}_2}{\partial x_1}\right). \end{aligned} \tag{11}$$

They are the three-dimensional analogue of the axial and shear forces of rod and MDOF models. The bimoments T_{11}, T_{22}, T_{12}, which are third-order moments of stress with no counterpart in classical theory, are

$$\begin{aligned} T_{11} &= \frac{1}{h^2}\int_{-h}^{h} \sigma_{11} z^3\, dz = \frac{H^2}{2}\left(E_{11}\frac{\partial \overline{\beta}_1}{\partial x_1} + E_{12}\frac{\partial \overline{\beta}_2}{\partial x_2} - E_{13}\frac{2(3\overline{\gamma} - \overline{W})}{H}\right), \\ T_{22} &= \frac{1}{h^2}\int_{-h}^{h} \sigma_{22} z^3\, dz = \frac{H^2}{2}\left(E_{12}\frac{\partial \overline{\beta}_1}{\partial x_1} + E_{22}\frac{\partial \overline{\beta}_2}{\partial x_2} - E_{23}\frac{2(3\overline{\gamma} - \overline{W})}{H}\right), \\ T_{12} &= T_{21} = \frac{1}{h^2}\int_{-h}^{h} \sigma_{12} z^3\, dz = \frac{H^2}{2} G_{12}\left(\frac{\partial \overline{\beta}_1}{\partial x_2} + \frac{\partial \overline{\beta}_2}{\partial x_1}\right). \end{aligned} \tag{12}$$

They measure the self-equilibrated, non-uniform part of the in-plane stresses across the width of the building (Figure 4, right). The transverse bimoments $\overline{p}_{13}, \overline{p}_{23}$ and the shear quantities $\overline{\tau}_{13}, \overline{\tau}_{23}$ are

$$\begin{aligned} \overline{p}_{13} &= G_{13}\left(\frac{\partial \overline{r}}{\partial x_1} + \frac{2(\overline{u}_1 - \overline{\psi}_1)}{H}\right), \quad \overline{\tau}_{13} = G_{13}\left(\frac{\partial \overline{\gamma}}{\partial x_1} + \frac{2(\overline{u}_1 - 3\overline{\beta}_1)}{H}\right), \\ \overline{p}_{23} &= G_{23}\left(\frac{\partial \overline{r}}{\partial x_2} + \frac{2(\overline{u}_2 - \overline{\psi}_2)}{H}\right), \quad \overline{\tau}_{23} = G_{23}\left(\frac{\partial \overline{\gamma}}{\partial x_2} + \frac{2(\overline{u}_2 - 3\overline{\beta}_2)}{H}\right), \end{aligned} \tag{13}$$

and the bimoments associated with σ_{33} are

$$\overline{p}_{33} = E_{31}\frac{\partial \overline{\psi}_1}{\partial x_1} + E_{32}\frac{\partial \overline{\psi}_2}{\partial x_2} + E_{33}\frac{2\overline{W}}{H}, \qquad \overline{\tau}_{33} = E_{31}\frac{\partial \overline{\beta}_1}{\partial x_1} + E_{32}\frac{\partial \overline{\beta}_2}{\partial x_2} + E_{33}\frac{2\overline{W} - 4\overline{r}}{H}. \tag{14}$$

Corrected Proof

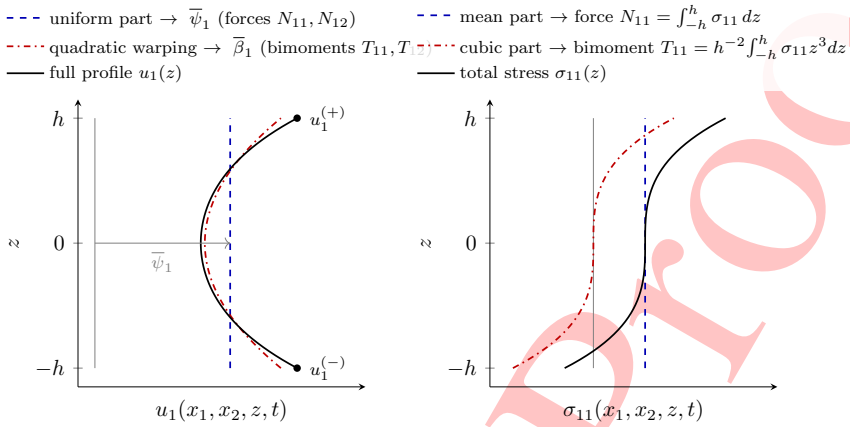

Figure 4: Through-thickness decomposition used in the bimoment theory: (left) the displacement $u_1(z)$ is represented by its mean value $\overline{\psi}_1$, its quadratic (warping) moment $\overline{\beta}_1$ and its face values $u_1^{(\pm)}$; (right) the stress $\sigma_{11}(z)$ gives the force N_{11} (mean part) and the bimoment T_{11} (self-equilibrated cubic part).

.

The face stresses $\overline{\sigma}_{11}, \overline{\sigma}_{12}, \overline{\sigma}_{22}$ that enter the contact conditions are

$$\begin{aligned}
\overline{\sigma}_{11} &= \left(E_{11}^0 - \frac{E_{13}^0}{E_{33}^0}\left(E_{31}^0 + G_{31}^0\right)\right)\frac{\partial \overline{u}_1}{\partial x_1} + \left(E_{12}^0 - \frac{E_{13}^0}{E_{33}^0}\left(E_{31}^0 + G_{31}^0\right)\right)\frac{\partial \overline{u}_2}{\partial x_2} + \frac{E_{13}^0}{E_{33}^0}\overline{q}_3, \\
\overline{\sigma}_{22} &= \left(E_{21}^0 - \frac{E_{23}^0}{E_{33}^0}\left(E_{32}^0 + G_{32}^0\right)\right)\frac{\partial \overline{u}_1}{\partial x_1} + \left(E_{22}^0 - \frac{E_{23}^0}{E_{33}^0}\left(E_{32}^0 + G_{32}^0\right)\right)\frac{\partial \overline{u}_2}{\partial x_2} + \frac{E_{23}^0}{E_{33}^0}\overline{q}_3, \\
\overline{\sigma}_{12} &= G_{12}^0\left(\frac{\partial \overline{u}_1}{\partial x_2} + \frac{\partial \overline{u}_2}{\partial x_1}\right),
\end{aligned} \tag{15}$$

where the superscript 0 refers to the elastic constants at the contact surface.

Finally, the local stresses between the longitudinal and transverse walls, denoted $\sigma_{13}^*, \sigma_{23}^*, \sigma_{33}^*$ to distinguish them from the averaged stresses (15), are

$$\begin{aligned}
\sigma_{13}^* &= G_{13}\left[\frac{210\left(9\overline{\beta}_1 - 2\overline{\psi}_1 - \overline{u}_1\right)}{H} - 30\frac{\partial \overline{W}}{\partial x_1}\right] + \frac{30}{H}\overline{q}_1 + \frac{\partial}{\partial x_1}\left(\frac{\overline{q}_3}{G_{13}}\right), \\
\sigma_{23}^* &= G_{23}\left[\frac{210\left(9\overline{\beta}_2 - 2\overline{\psi}_2 - \overline{u}_2\right)}{H} - 30\frac{\partial \overline{W}}{\partial x_2}\right] + \frac{30}{H}\overline{q}_2 + \frac{\partial}{\partial x_2}\left(\frac{\overline{q}_3}{G_{23}}\right), \\
\sigma_{33}^* &= E_{33}\frac{210\left(33\overline{\gamma} - 9\overline{W} - 4\overline{r}\right)}{H} - \frac{42}{H}E_{31}\frac{\partial \overline{u}_1}{\partial x_1} - \frac{42}{H}E_{32}\frac{\partial \overline{u}_2}{\partial x_2} - E_{31}\frac{\partial^2 \overline{W}}{\partial x_1^2} - E_{32}\frac{\partial^2 \overline{W}}{\partial x_2^2} \\
&\quad + \frac{42}{H}\overline{q}_3 + E_{31}\frac{\partial}{\partial x_1}\left(\frac{\overline{q}_1}{G_{13}}\right) + E_{32}\frac{\partial}{\partial x_2}\left(\frac{\overline{q}_2}{G_{23}}\right).
\end{aligned} \tag{16}$$

Forces N_{ij} are measured in N/m, bimoments T_{ij} in N, and the quantities $\overline{p}_{ij}, \overline{\tau}_{ij}$, the face stresses $\overline{\sigma}_{ij}$ and the local stresses σ_{ij}^* in Pa.

Corrected Proof

4 Equations of motion, boundary and contact conditions

The equations of motion [21, 26] consist of three systems. The first system contains the equations of longitudinal and tangential forces:

$$\begin{gathered}\frac{\partial N_{11}}{\partial x_1}+\frac{\partial N_{12}}{\partial x_2}+\frac{2}{H}\overline{q}_1=\rho\,\ddot{\overline{\psi}}_1,\\ \frac{\partial N_{21}}{\partial x_1}+\frac{\partial N_{22}}{\partial x_2}+\frac{2}{H}\overline{q}_2=\rho\,\ddot{\overline{\psi}}_2,\\ \frac{\partial \overline{\tau}_{13}}{\partial x_1}+\frac{\partial \overline{\tau}_{23}}{\partial x_2}-\frac{6}{H}\overline{\tau}_{33}+\frac{2}{H}\overline{q}_3=\rho\,\ddot{\overline{\gamma}}.\end{gathered} \tag{17}$$

When all bimoment terms vanish, (17) reduces to the equation of longitudinal motion of a rod or shear beam. The second system contains the equations of longitudinal and tangential bimoments:

$$\begin{gathered}\frac{\partial T_{11}}{\partial x_1}+\frac{\partial T_{12}}{\partial x_2}-\frac{4}{H}\overline{p}_{13}+\frac{2}{H}\overline{q}_1=\rho\,\ddot{\overline{\beta}}_1,\\ \frac{\partial T_{12}}{\partial x_1}+\frac{\partial T_{22}}{\partial x_2}-\frac{4}{H}\overline{p}_{23}+\frac{2}{H}\overline{q}_2=\rho\,\ddot{\overline{\beta}}_2,\\ \frac{\partial \overline{p}_{13}}{\partial x_1}+\frac{\partial \overline{p}_{23}}{\partial x_2}-\frac{2}{H}\overline{p}_{33}+\frac{2}{H}\overline{q}_3=\rho\,\ddot{\overline{r}}.\end{gathered} \tag{18}$$

This system governs the warping functions $\overline{\beta}_1, \overline{\beta}_2, \overline{r}$ and has no counterpart in beam and MDOF theories. The third system contains the equations of longitudinal and compressive bimoments:

$$\begin{gathered}\frac{\partial \overline{\sigma}_{11}}{\partial x_1}+\frac{\partial \overline{\sigma}_{12}}{\partial x_2}+\frac{\sigma^*_{13}}{H}=\rho\,\ddot{\overline{u}}_1,\\ \frac{\partial \overline{\sigma}_{21}}{\partial x_1}+\frac{\partial \overline{\sigma}_{22}}{\partial x_2}+\frac{\sigma^*_{23}}{H}=\rho\,\ddot{\overline{u}}_2,\\ \frac{\partial \overline{q}_1}{\partial x_1}+\frac{\partial \overline{q}_2}{\partial x_2}+\frac{\sigma^*_{33}}{H}=\rho\,\ddot{\overline{W}}.\end{gathered} \tag{19}$$

No damping terms enter (17)–(19); all finite-difference results of this paper therefore refer to the undamped system.

On the free lateral faces $x_1 = 0, a$ of the building,

$$N_{11}=N_{12}=0,\quad T_{11}=T_{12}=0,\quad \overline{p}_{13}=\overline{\tau}_{13}=0,\quad \overline{\sigma}_{11}=\overline{\sigma}_{12}=0,\quad \sigma^*_{13}=0, \tag{20}$$

and on the free top face $x_2 = b$,

$$N_{12}=N_{22}=0,\quad T_{12}=T_{22}=0,\quad \overline{p}_{23}=\overline{\tau}_{23}=0,\quad \overline{\sigma}_{12}=\overline{\sigma}_{22}=0,\quad \sigma^*_{23}=0. \tag{21}$$

On the lateral faces of the foundation embedded in the soil, the stress factors are equal to those transmitted by the soil (superscript *gr*):

$$\begin{gathered}N_{11}=N^{gr}_{11},\ N_{12}=N^{gr}_{12},\ T_{11}=T^{gr}_{11},\ T_{12}=T^{gr}_{12},\ \overline{p}_{13}=p^{gr}_{13},\ \overline{\tau}_{13}=\tau^{gr}_{13},\\ \overline{\sigma}_{11}=\sigma^{gr}_{11},\ \overline{\sigma}_{12}=\sigma^{gr}_{12},\ \sigma^*_{13}=\sigma^{gr}_{13},\end{gathered} \tag{22}$$

Corrected Proof

and on the horizontal foundation–soil surfaces

$$N_{12}=N_{12}^{gr},\ N_{22}=N_{22}^{gr},\ T_{12}=T_{12}^{gr},\ T_{22}=T_{22}^{gr},\ \overline{p}_{23}=p_{23}^{gr},\ \overline{\tau}_{23}=\tau_{23}^{gr},\\ \overline{\sigma}_{12}=\sigma_{12}^{gr},\ \overline{\sigma}_{22}=\sigma_{22}^{gr},\ \sigma_{23}^{*}=\sigma_{23}^{gr}. \tag{23}$$

Conditions (20)–(21) express traction-free faces, while (22)–(23) express the continuity of forces and bimoments at Γ_{fs} and introduce the compliance of the soil into the model; this is the point where the present formulation differs from the rigid-base models of [17, 27, 31].

At the building–foundation surface Γ_{bf} the conjugation conditions are

$$\overline{\psi}_1=\overline{\psi}_1^{(0)},\quad \overline{\psi}_2=\overline{\psi}_2^{(0)},\quad \overline{\beta}_1=\tfrac{1}{3}\overline{\beta}_1^{(0)},\quad \overline{\beta}_2=\tfrac{1}{3}\overline{\beta}_2^{(0)},\\ \overline{u}_1=\overline{u}_1^{(0)},\quad \overline{u}_2=\overline{u}_2^{(0)},\quad \overline{r}=\overline{r}^{(0)},\quad \overline{\gamma}=\overline{\gamma}^{(0)},\quad \overline{W}=\overline{W}^{(0)}, \tag{24}$$

where the superscript (0) denotes the generalized displacements of the upper surface of the foundation. The factor $1/3$ results from the different through-thickness weighting of the foundation slab and of the building story bonded to it.

5 Numerical method: finite-difference discretization and stability

The problem of Sections 3–4 is solved by the finite-difference method on a uniform mesh in $x_1\in[0,a]$, $x_2\in[0,b]$ with steps

$$\Delta x_1=\frac{a}{N},\qquad \Delta x_2=\frac{b}{M}, \tag{25}$$

nodes (i,j), $i=0,\dots,N$, $j=0,\dots,M$. First derivatives of the generalized displacements are approximated by central differences,

$$\left(\frac{\partial f}{\partial x_1}\right)_{i,j}=\frac{f_{i+1,j}-f_{i-1,j}}{2\Delta x_1},\qquad \left(\frac{\partial f}{\partial x_2}\right)_{i,j}=\frac{f_{i,j+1}-f_{i,j-1}}{2\Delta x_2}, \tag{26}$$

and derivatives of the stress factors $F=N_{ij},T_{ij},\overline{p}_{ij},\overline{\tau}_{ij}$ by central differences on half-steps,

$$\frac{\partial F_{i,j}^{k}}{\partial x_1}=\frac{F_{i+\frac12,j}^{k}-F_{i-\frac12,j}^{k}}{\Delta x_1},\qquad \frac{\partial F_{i,j}^{k}}{\partial x_2}=\frac{F_{i,j+\frac12}^{k}-F_{i,j-\frac12}^{k}}{\Delta x_2}, \tag{27}$$

where k is the time level. The second time derivative is approximated by the explicit central-difference formula

$$\frac{\partial^2 f_{i,j}^{k}}{\partial t^2}=\frac{f_{i,j}^{k+1}-2f_{i,j}^{k}+f_{i,j}^{k-1}}{\Delta t^2}. \tag{28}$$

Substituting (26)–(28) into (17)–(19) gives explicit formulas for $f_{i,j}^{k+1}$ in terms of values at levels k and $k-1$; no matrix has to be inverted. The algorithm is implemented in the authors' program for the dynamic calculation of multistory buildings based on the bimoment theory of plates, registered by the Ministry of Justice of the Republic of Uzbekistan (certificate No. DGU 68846, 22.09.2026).

Corrected Proof

Table 2: Mesh and time-stepping parameters

Parameter	Value
Mesh, $N \times M$	30×56
Mesh steps, $\Delta x_1 = a/N$, $\Delta x_2 = b/M$	≈ 1 m
Stability factor, $\min(k_1, k_2)$	≥ 4
Time step, Δt	eq. (30) with $k_1 = k_2 = 4$
Number of time steps	up to 6.5×10^4
Truncation error	$O(\Delta x_1^2 + \Delta x_2^2 + \Delta t^2)$
Damping	none (undamped)

The explicit scheme is stable if the time step satisfies the Courant–Friedrichs–Lewy condition [8], which for the two-dimensional mesh reads

$$c\,\Delta t \sqrt{\frac{1}{\Delta x_1^2} + \frac{1}{\Delta x_2^2}} \leq 1, \qquad c = \max\Big(\sqrt{E_1/\rho}, \sqrt{E_2/\rho}\Big), \tag{29}$$

where c (m/s) is the largest longitudinal wave speed of the continual model. In the computations

$$\frac{c\,\Delta t}{\Delta x_1} = \frac{1}{k_1}, \qquad \frac{c\,\Delta t}{\Delta x_2} = \frac{1}{k_2}, \qquad \min(k_1, k_2) \geq 4, \tag{30}$$

so that the left-hand side of (29) does not exceed $\sqrt{2}/4 \approx 0.35$, i.e. the time step is about three times smaller than the stability limit, which keeps the phase error small over the long computations needed to resolve the beating near resonance (Section 6). The parameters are listed in Table 2.

Input data. The walls are made of reinforced concrete with $E_0 = 25{,}000$ MPa, $\rho_0 = 2500$ kg/m^3 and $\nu_w = 0.25$. The elastic characteristics of the foundation and soil and the geometric characteristics of the rooms and of the building are prescribed as input data.

6 Results: natural frequencies, time histories and frequency response

The ground motion acts along the axis Ox_1 (the length of the building) with the base acceleration

$$\ddot{u}_0(t) = a_0 \cos(\omega_0 t), \tag{31}$$

where $a_0 = k_c g$ (m/s^2, $g = 9.81$ m/s^2) is the peak ground acceleration, k_c is the seismic coefficient, ν_0 (Hz) is the excitation frequency and $\omega_0 = 2\pi\nu_0$ (rad/s) the corresponding angular frequency. Throughout the paper frequencies denoted by ν or p are ordinary frequencies in Hz, and frequencies denoted by ω or $\hat{p}$ are angular frequencies in rad/s. Integrating (31) twice with zero initial displacement and velocity gives

$$u_0(t) = \frac{a_0}{\omega_0^2}\big(1 - \cos(\omega_0 t)\big) = \frac{A_0}{2}\big(1 - \cos(\omega_0 t)\big), \qquad A_0 = \frac{2a_0}{\omega_0^2} = \frac{2k_c g}{\omega_0^2}. \tag{32}$$

Thus A_0 is the *maximum ground displacement*: the base oscillates between 0 and A_0 (amplitude $A_0/2$ about the mean position $A_0/2$), its velocity $(a_0/\omega_0)\sin(\omega_0 t)$ starts from zero, and its acceleration is exactly (31). The coefficients $k_c = 0.1, 0.2, 0.4$ correspond to seismic intensities 7, 8 and 9 on the MSK-64 scale. For $k_c = 0.2$ and $\nu_0 = 3$ Hz ($a_0 = 1.962$ m/s^2, $\omega_0 = 18.85$ rad/s), (32) gives $A_0 = 1.10$ cm.

Corrected Proof

Table 3: Models and damping assumptions of the reported results

Result	Model	Damping
Natural frequencies and periods (Tables 4, 5)	FD model	none
Peak roof displacements (Table 6)	FD model	none
Stress growth near resonance (Section 6.5)	FD model	none
Beating near resonance (Figure 5a)	modal model (34)	$\zeta = 0$
Forced vibration at 3 Hz (Figure 5b)	modal model (34)	$\zeta = 0.05$
Frequency response (Figure 6)	modal model (35)	$\zeta = 0.05$; 0.02
1D fixed-base comparison, 2.2–2.5 cm (Section 7.2)	modal model (34)	$\zeta = 0$

Table 4: First three natural frequencies (Hz) of a 16-story building (undamped FD model)

Stories	H, m	p_1, Hz	p_2, Hz	p_3, Hz
16	13	1.950	7.495	16.09
	15	1.850	7.201	15.50
	18	1.725	6.993	14.80

6.1 Models and damping assumptions

Two models are used in this section, and they differ in their damping assumptions. (a) The *finite-difference (FD) model* of Sections 3–5 is undamped; it gives the natural frequencies (Tables 4 and 5), the peak displacements (Table 6) and the stress behaviour near resonance (Section 6.5). (b) The *modal model* (34) uses the natural frequencies obtained from the FD model and is used only to present time histories and frequency responses; it is evaluated without damping ($\zeta = 0$) and with the damping ratios $\zeta = 0.05$ (a value commonly adopted for reinforced-concrete buildings [6]) and $\zeta = 0.02$. Table 3 indicates which result corresponds to which model.

6.2 Natural frequencies

The natural frequencies were found by the resonance method. The excitation frequency ν_0 is increased step by step, and for each value the undamped FD problem is integrated over the same time interval $[0, t_{\max}]$ (Table 2); the peak roof displacement

$$U_{\max}(\nu_0) = \max_{0 \le t \le t_{\max}} \left| \bar{u}_1(x_1, b, t) \right| \tag{33}$$

is recorded. When ν_0 approaches a natural frequency, the response of the undamped system grows with time (beating with the period $1/|p_k - \nu_0|$, Section 6.3), so that $U_{\max}(\nu_0)$ has a sharp local maximum. The natural frequency p_k is taken as the value of ν_0 at which this local maximum occurs, the step in ν_0 being refined near each peak. Because the computation interval is finite, the computed response remains finite: resonance appears as a large resonant growth of the response, not as a mathematically unbounded one, and the frequency resolution of the method is of the order of $1/t_{\max}$. Table 4 lists the first three natural frequencies of a 16-story building for $H = 13$, 15 and 18 m, and Table 5 the corresponding periods.

Corrected Proof

Table 5: Natural periods $T_k = 1/p_k$ corresponding to Table 4

H, m	T_1, s	T_2, s	T_3, s
13	0.513	0.133	0.0622
15	0.541	0.139	0.0645
18	0.580	0.143	0.0676

All three frequencies decrease as the width increases from 13 to 18 m; p_1 falls from 1.950 to 1.725 Hz. A wider building has a larger mass per unit length of the plate without a proportional increase of its in-plane stiffness.

6.3 Time histories

To present the dynamic response in the time and frequency domains, the first three modes identified above are used in a modal representation of the roof displacement relative to the base,

$$u_{\text{roof}}(t) - u_0(t) = \sum_{k=1}^{3} \Gamma_k \phi_k(b)\, q_k(t), \qquad \ddot{q}_k + 2\zeta \hat{p}_k \dot{q}_k + \hat{p}_k^2 q_k = -\ddot{u}_0(t), \qquad q_k(0) = \dot{q}_k(0) = 0, \quad (34)$$

where $\hat{p}_k = 2\pi p_k$ (rad/s) are the angular natural frequencies corresponding to p_k (Hz) of Table 4, ζ is the damping ratio and $\Gamma_k \phi_k(b) = 4(-1)^{k+1}/[(2k-1)\pi]$ are the roof participation factors of a uniform shear cantilever [6]. Equations (34) were integrated in closed form.

Figure 5(a) shows the roof response of the building with $H = 15$ m for $k_c = 0.2$ and $\nu_0 = 1.70$ Hz $\approx 0.92\, p_1$ without damping. The response exhibits beating with the period $1/(p_1 - \nu_0) \approx 6.7$ s, and the envelope of the first-mode response, $2a_0\Gamma_1\phi_1(b)/|\hat{p}_1^2 - \omega_0^2|$, reaches 23.8 cm. As ν_0 approaches p_1, both the beat period and the envelope increase in inverse proportion to the frequency mismatch $|p_1 - \nu_0|$; within any finite time interval the response remains finite but becomes large. The same resonant growth is observed in the FD computations used to identify the natural frequencies (Section 6.2). Figure 5(b) shows the response at $\nu_0 = 3.0$ Hz and $k_c = 0.2$ with $\zeta = 0.05$ for the three widths: after a transient of about 3 s the roof oscillates with the excitation frequency and an amplitude of 1.25, 1.17 and 1.09 cm relative to the base for $H = 13$, 15 and 18 m.

6.4 Frequency response

The steady-state amplitude of (34) is

$$U(\nu_0) = a_0 \left| \sum_{k=1}^{3} \frac{\Gamma_k \phi_k(b)}{\hat{p}_k^2 - \omega_0^2 + 2\mathrm{i}\,\zeta \hat{p}_k \omega_0} \right|, \qquad \omega_0 = 2\pi\nu_0. \quad (35)$$

Figure 6 shows $U(\nu_0)$ for $k_c = 0.2$. The first resonance dominates: with $\zeta = 0.05$ the peak amplitude is 16.7, 18.5 and 21.3 cm for $H = 13$, 15 and 18 m, and with $\zeta = 0.02$ it is 46 cm for $H = 15$ m. For $H = 15$ m and $\zeta = 0.05$ the second and third peaks are about 0.4 cm and 0.05 cm, i.e. more than an order of magnitude lower. The first natural frequencies of all three buildings lie inside the band 1.4–4.0 Hz of dominant frequencies of earthquakes in Uzbekistan (shaded in Figure 6); at $\nu_0 = 3$ Hz the steady amplitude is 1.09–1.25 cm, in agreement with Figure 5(b).

Corrected Proof

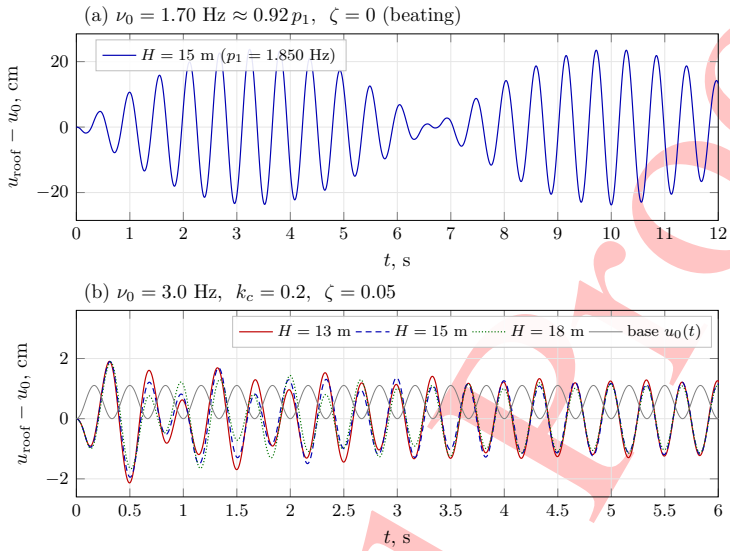

Figure 5: Time histories of the roof displacement relative to the base for a 16-story building (modal model (34)): (a) beating near resonance, $H = 15$ m, $k_c = 0.2$, $\nu_0 = 1.70$ Hz, no damping ($\zeta = 0$); (b) forced vibration at $\nu_0 = 3.0$ Hz, $k_c = 0.2$, $\zeta = 0.05$, for $H = 13$, 15 and 18 m, together with the base displacement $u_0(t)$ of eq. (32)

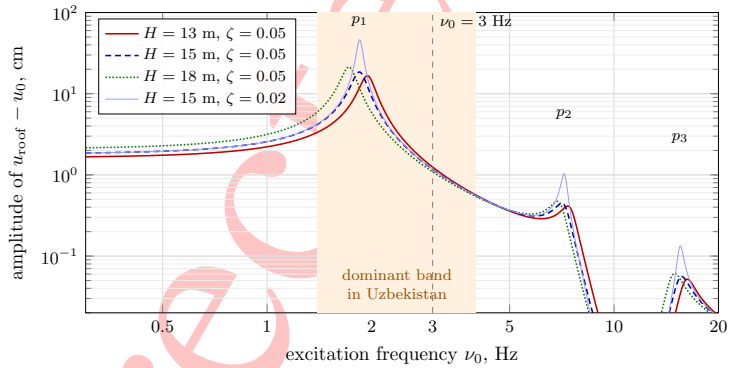

Figure 6: Frequency response of the roof displacement relative to the base of a 16-story building, $k_c = 0.2$, eq. (35) (modal model, damping ratios as indicated). The shaded band is the range of dominant frequencies of earthquakes in Uzbekistan; p_1, p_2, p_3 are the natural frequencies for $H = 15$ m.

6.5 Displacements and stresses

Table 6 gives the peak roof displacements computed with the full undamped finite-difference model at $k_c = 0.2$ and $\nu_0 = 3.0$ Hz; the peak values are taken over the whole computation interval and include the transient part of the response. The horizontal displacement $\overline{u}_1$ at the two corner points of the roof is 5.0 and 4.5 cm. The vertical displacement $\overline{u}_2$ is 1.1–1.2 cm at the corners and does not exceed 0.08 cm at the middle of the roof; this antisymmetric pattern shows rocking of the building on the compliant foundation, which a planar or fixed-base model cannot describe.

When the excitation frequency is swept through 1.2–4.5 Hz and approaches the natural frequencies of the building–foundation system, the normal stress σ_{22} in the 16-story building shows a strong resonant

Corrected Proof

Table 6: Peak roof displacements of a 16-story building ($H = 15$ m) at $k_c = 0.2$, $\nu_0 = 3.0$ Hz (undamped finite-difference model)

Quantity	Value
Horizontal displacement $\overline{u}_1$, corner points of the roof	4.5–5.0 cm
Vertical displacement $\overline{u}_2$, corner points of the roof	1.1–1.2 cm
Vertical displacement $\overline{u}_2$, middle of the roof	≤ 0.08 cm

growth in the lower stories and in the contact zone with the foundation. Because the FD model contains no damping, the stresses obtained near resonance depend on the length of the computation interval and represent an upper (undamped) bound; they are therefore not used as quantitative design values.

7 Comparison with code estimates, a one-dimensional model and the literature

7.1 Natural periods

Table 7 compares the computed fundamental periods with approximate code formulas. These formulas are empirical expressions for the design period and serve here as a comparative reference, not as a validation of the continual model. The following expressions and assumptions were used.

Eurocode 8 [10], EN 1998-1, clause 4.3.3.2.2(3):

$$\begin{gathered} T_1 = C_t\, b^{3/4}, \\ C_t = 0.050 \quad \text{(structures other than moment-resisting frames)}, \\ C_t = \frac{0.075}{\sqrt{A_c}} \quad \text{(concrete or masonry shear walls)}, \end{gathered} \tag{36}$$

with $A_c = \sum_i A_i\,(0.2 + l_{wi}/b)^2$ (m^2), where A_i is the effective cross-sectional area and l_{wi} ($l_{wi}/b \leq 0.9$) the length of the i-th shear wall in the first story in the direction considered, and b is the building height in m.

ASCE/SEI 7-16 [3], Eq. (12.8-7) in SI units:

$$T_a = C_t\, b^x, \qquad C_t = 0.0488, \quad x = 0.75 \text{ (“all other structural systems”)}. \tag{37}$$

Assumptions. The building is a reinforced-concrete bearing-wall (box-type) structure with $N_s = 16$ and story height $b_1 = 3.0$–3.5 m, so that $b = 48$–56 m; the vibration direction is Ox_1, so the walls parallel to Ox_1 (longitudinal walls A, B, C in Figure 2) are the shear walls in (36). The generic expressions ($C_t = 0.050$ and $C_t = 0.0488$) treat the building as an “other” structure and ignore its dense wall system; they give 0.89–1.02 s. For the wall expression, A_c was not computed from a specific wall layout; instead, the range $A_c = 6$–8 m^2, which is of the order expected for three longitudinal walls with openings, was taken, giving 0.48–0.63 s. Conversely, the computed periods 0.513–0.580 s correspond to $A_c \approx 5.6$–9.0 m^2. Note that EN 1998-1 gives (36) for buildings up to 40 m high, so for $b = 48$–56 m it is used beyond its formal range of application. The comparison therefore shows only that the computed periods are of the same order as the code estimate for wall buildings and much shorter than the generic estimates,

Corrected Proof

Table 7: Fundamental period of the 16-story building: present model versus code formulas (reference values)

Source	T_1, s
Present plate model with foundation and soil (H = 13–18 m)	0.513–0.580
Eurocode 8, $C_t = 0.05$, b = 48–56 m, eq. (36) [10]	0.91–1.02
ASCE/SEI 7-16, $C_t = 0.0488$, $x = 0.75$, b = 48–56 m, eq. (37) [3]	0.89–1.00
Eurocode 8, walls, $C_t = 0.075/\sqrt{A_c}$, A_c = 6–8 m^2, b = 48–56 m [10]	0.48–0.63

as expected for stiff box-type buildings. Ambient-vibration surveys of reinforced-concrete buildings in Europe [11, 18] have shown that measured periods depend mainly on height or number of stories and differ considerably from code provisions, with large scatter.

Our earlier rigid-base analysis [27] gave $T_1 = 0.20$ s for a 12-story building with $H = 13$ m and $E_0 = 20{,}000$ MPa. Since the number of stories and the material constants differ, this comparison is only qualitative: the present periods are much longer than this value would suggest for a 16-story building, which is consistent with the period lengthening due to foundation compliance known from SSI studies [15, 25, 35].

7.2 Comparison with a classical one-dimensional model

The modal model (34) with the same frequencies is a fixed-base one-dimensional model of the Chopra type [6]. Without damping, at $k_c = 0.2$ and $\nu_0 = 3$ Hz it gives a peak roof displacement relative to the base of 2.50, 2.33 and 2.18 cm for $H = 13$, 15 and 18 m (transient included, $0 \le t \le 20$ s). Adding the maximum base displacement $A_0 = 1.10$ cm gives an upper bound of 3.6 cm for the absolute roof displacement of this model, whereas the plate model gives 4.5–5.0 cm at the corner points (Table 6). The difference is explained by effects absent from the one-dimensional model: the rocking of the building on the compliant foundation, shown by the corner vertical displacements of 1.1–1.2 cm, and the variation of the displacement over the plan. A one-dimensional model gives one value per level and cannot distinguish corner and middle points.

7.3 Effect of bimoments and of the foundation

The two features that distinguish the present model from the classical ones are visible directly in the results of Sections 6.5 and 7.2. First, the compliant foundation produces a rocking of the building: the vertical roof displacement is 1.1–1.2 cm at the corner points but does not exceed 0.08 cm at the middle (Table 6), and the horizontal corner displacement (4.5–5.0 cm) exceeds the upper bound 3.6 cm of the fixed-base one-dimensional model. With a rigid base, $\overline{u}_1(x_1, 0, t) = u_0(t)$ as in [27, 31], this rocking mode is suppressed. Second, the bimoment system (18) governs the warping functions $\overline{\beta}_1, \overline{\beta}_2, \overline{r}$, which are excluded by the plane-section hypothesis of beam and shear-type MDOF models [6, 20]; the warping is largest near the foundation, where the contact conditions (24) constrain the cross-section, and it contributes to the normal stress σ_{22} through the bimoments T_{22} and $\overline{\tau}_{33}$ of (12) and (14). A quantitative comparison of the stresses obtained with the full model, with the bimoment terms removed and with a

Corrected Proof

rigid base, computed for the same building and excitation, is planned as a separate study.

8 Conclusions

A spatial continual plate model based on the bimoment theory of thick plates has been developed for the longitudinal seismic vibrations of box-type multistory buildings coupled to a slab foundation and a compliant soil base. The main results are as follows.

1. Closed-form reduced elastic moduli, shear moduli and density of the continual model have been obtained from the cellular wall–slab geometry; the reduced moduli are 10–30 times and the reduced density 8–15 times smaller than those of the wall material.
2. A complete boundary-value problem has been formulated: three coupled systems of equations for forces, bimoments and compressive bimoments in nine generalized displacements, conditions on the free faces, and contact conditions at the building–foundation and foundation–soil interfaces. Unlike the earlier plate-model studies [17, 27, 29, 31], the base is not rigid.
3. The undamped problem is solved by an explicit finite-difference scheme whose time step is about three times smaller than the two-dimensional Courant–Friedrichs–Lewy limit (29).
4. For 16-story buildings with $H = 13$–18 m the first natural frequency is 1.95–1.73 Hz ($T_1 = 0.51$–0.58 s), of the same order as the Eurocode 8 estimate for wall buildings (0.48–0.63 s, Table 7), which serves as a reference value rather than a validation. These frequencies lie in the band 1.4–4.0 Hz typical of earthquakes in Uzbekistan.
5. Time histories show resonant growth (beating) near resonance and a steady forced response at 3 Hz; the frequency response is dominated by the first mode.
6. At $k_c = 0.2$, $\nu_0 = 3$ Hz the horizontal roof displacement is 4.5–5.0 cm at the corners and the vertical displacement 1.1–1.2 cm at the corners but below 0.08 cm at the middle, a rocking pattern that a fixed-base one-dimensional model, which gives 2.2–2.5 cm relative to the base, cannot capture.
7. The compliant foundation produces a rocking of the building that a fixed-base model cannot describe, and the bimoment equations describe the warping of the cross-section near the foundation, which is excluded by the plane-section hypothesis of classical models.

Foundation stiffness, mass and geometry significantly influence the natural frequencies of the building–foundation system and should therefore be considered in resonance assessment. Since the present model does not include damping or nonlinear behaviour of the materials and soil, the computed resonant amplitudes and stresses are upper bounds and are not intended as direct design values. Future work will include damping, irregular plans, nonlinear behaviour of the materials and soil, buildings with a larger number of stories, a quantitative stress comparison with rigid-base and bimoment-free models, and comparison with measurements on real buildings.

Author contributions

M.K. Usarov: conceptualisation, methodology, theoretical formulation, supervision. B.M. Kamalov: numerical implementation, software, data curation. D.K. Shamsiyev: validation, formal analysis, visualisation. Y.S. Khurramov: investigation, writing – review and editing. All authors have read and agreed to the published version of the manuscript.

Corrected Proof

Funding

This research was carried out within the fundamental research programme of the Institute of Mechanics and Seismic Stability of Structures named after M.T. Urazbaev, Academy of Sciences of the Republic of Uzbekistan.

Conflict of interest

The authors declare no conflict of interest.

References

[1] Z.K. Abaev, M.Yu. Kodzaev, A.A. Bigulaev, *Earthquake resistance analysis of structural systems of multi-storey civil buildings*, Struct. Mech. Eng. Constr. Build. **16** (2020) 76–82.

[2] S.E. Abdel Raheem, M.M.M. Ahmed, M.M. Ahmed, A.G.A. Abdel-shafy, *Evaluation of plan configuration irregularity effects on seismic response demands of L-shaped MRF buildings*, Bull. Earthq. Eng. **16** (2018) 3845–3869.

[3] American Society of Civil Engineers, *Minimum Design Loads and Associated Criteria for Buildings and Other Structures*, ASCE/SEI 7-16, ASCE, Reston, VA, 2017.

[4] G.T. Ayubov, G.I. Mamatisaev, F.A. Usanov, S.I. Askarhodjaev, B. Urinov, *Estimation of seismic resistance of multi-storey buildings based on a continuum model*, E3S Web Conf. **402** (2023) 07019.

[5] A. Chakraborty, K. Bhattacharya, V.A. Sawant, *Soil structure interaction effects on multistorey asymmetric building subjected to earthquake loading*, Indian Geotech. J. **55** (2025) 303–314.

[6] A.K. Chopra, *Dynamics of Structures: Theory and Applications to Earthquake Engineering*, 5th ed., Pearson, Hoboken, 2017.

[7] R.W. Clough, J. Penzien, *Dynamics of Structures*, 3rd ed., Computers & Structures, Berkeley, 2003.

[8] R. Courant, K. Friedrichs, H. Lewy, *Über die partiellen Differenzengleichungen der mathematischen Physik*, Math. Ann. **100** (1928) 32–74.

[9] S.A. El-Betar, *Seismic vulnerability evaluation of existing R.C. buildings*, HBRC J. **14** (2018) 189–197.

[10] European Committee for Standardization, *Eurocode 8: Design of Structures for Earthquake Resistance – Part 1: General Rules, Seismic Actions and Rules for Buildings*, EN 1998-1:2004, CEN, Brussels, 2004.

[11] M.R. Gallipoli, M. Mucciarelli, B. Šket-Motnikar, et al., *Empirical estimates of dynamic parameters on a large set of European buildings*, Bull. Earthq. Eng. **8** (2010) 593–607.

Corrected Proof

[12] A. Ghersi, P.P. Rossi, *Influence of bi-directional ground motions on the inelastic response of one-storey in-plan irregular systems*, Eng. Struct. **23** (2001) 579–591.

[13] C.C. Ike, *A third-order shear deformation plate bending formulation for thick plates: first principles derivation and applications*, Math. Models Eng. **9** (2023) 144–168.

[14] S.B. KC, L. Zhang, G. Wang, *Ground-motion modification by soil, structures, and topography: a review of soil structure interaction (SSI) and its multi-scale extensions*, Buildings **15** (2025) 4170.

[15] S. Khan, S. Alam, S. Alam, A.B. Nabilah, M.T. Naqash, *Effect of soil-structure interaction on the seismic response of a building with combined bracing and shear wall*, Structures **84** (2026) 110985.

[16] S.G. Lekhnitskii, *Theory of Elasticity of an Anisotropic Body*, Mir Publishers, Moscow, 1981.

[17] G.I. Mamatisaev, D.K. Shamsiev, S.I. Askarhodjaev, M.Sh. Kurbanbaev, J.A. Yarashov, *To the solution of the problem of longitudinal vibrations of multi-storey buildings on the basis of the plate model*, E3S Web Conf. **402** (2023) 07018.

[18] C. Michel, P. Guéguen, P. Lestuzzi, P.-Y. Bard, *Comparison between seismic vulnerability models and experimental dynamic properties of existing buildings in France*, Bull. Earthq. Eng. **8** (2010) 1295–1307.

[19] R.D. Mindlin, *Influence of rotatory inertia and shear on flexural motions of isotropic, elastic plates*, J. Appl. Mech. **18** (1951) 31–38.

[20] E. Miranda, S. Taghavi, *Approximate floor acceleration demands in multistory buildings. I: Formulation*, J. Struct. Eng. **131** (2005) 203–211.

[21] M. Mirsaidov, M. Usarov, *Bimoment theory construction to assess the stress state of thick orthotropic plates*, IOP Conf. Ser. Earth Environ. Sci. **614** (2020) 012090.

[22] J.N. Reddy, *A simple higher-order theory for laminated composite plates*, J. Appl. Mech. **51** (1984) 745–752.

[23] A.B. Rigato, R.A. Medina, *Influence of angle of incidence on seismic demands for inelastic single-storey structures subjected to bi-directional ground motions*, Eng. Struct. **29** (2007) 2593–2601.

[24] B. Stafford Smith, A. Coull, *Tall Building Structures: Analysis and Design*, Wiley, New York, 1991.

[25] J.P. Stewart, G.L. Fenves, R.B. Seed, *Seismic soil-structure interaction in buildings. I: Analytical methods*, J. Geotech. Geoenviron. Eng. **125** (1999) 26–37.

[26] M.K. Usarov, *Bimoment Theory of Thick Anisotropic Plates*, Fan Ziyosi, Tashkent, 2022 (in Russian).

[27] M. Usarov, G. Isaev, D. Shamsiev, M. Kurbanbaev, E. Toshmatov, *Seismic resistance calculation in multi-story structures under vibration forces*, E3S Web Conf. **583** (2024) 06006.

Corrected Proof

[28] M.K. Usarov, G.I. Mamatisaev, J. Yarashov, E. Toshmatov, *Non-stationary oscillations of a box-like structure of a building*, in: Modern Methods of Structural Analysis, Moscow State University of Civil Engineering, Moscow, 2019, pp. 130–139.

[29] M. Usarov, F. Usanov, S. Askarhodjaev, *Seismic vibrations of multi-storey buildings within the framework of the plate model*, AIP Conf. Proc. **3177** (2025) 050019.

[30] M.K. Usarov, D. Usarov, F. Usanov, S. Askarhodjaev, J. Yarashov, *Dynamic analysis of displacement and stress in multi-story structures under transverse vibrations*, E3S Web Conf. **583** (2024) 06007.

[31] M.K. Usarov, D.M. Usarov, G.U. Isaev, M.Sh. Kurbanbaev, B. Yuldoshev, *Estimation of seismic resistance of multi-story buildings in the framework of the bimoment theory using the plate model*, E3S Web Conf. **402** (2023) 07017.

[32] F. Vicencio, N.A. Alexander, C. Málaga-Chuquitaype, *Seismic structure-soil-structure interaction between inelastic structures*, Earthq. Eng. Struct. Dyn. **53** (2024) 1446–1464.

[33] V.Z. Vlasov, *Thin-Walled Elastic Beams*, 2nd ed., Israel Program for Scientific Translations, Jerusalem, 1961.

[34] J. Wdowicki, E. Wdowicka, Z. Pawlak, *Dynamic analysis of irregular multistorey shear wall buildings using continuous-discrete approach*, in: Z. Zembaty, M. De Stefano (Eds.), Seismic Behaviour and Design of Irregular and Complex Civil Structures II, Springer, Cham, 2016, pp. 263–274.

[35] J.P. Wolf, *Dynamic Soil-Structure Interaction*, Prentice-Hall, Englewood Cliffs, NJ, 1985.

Corrected Proof